

Visible resonant modes in GaN-based photonic crystal membrane cavities

Cedrik Meier^{a)}

Departments of Materials and Electrical & Computer Engineering, University of California—Santa Barbara, Santa Barbara, California 93106 and University of Duisburg—Essen, Experimental Physics, Lotharstr. 1, D-47048 Duisburg, Germany

Kevin Hennessy, Elaine D. Haberer, Rajat Sharma, Yong-Seok Choi, Kelly McGroddy, Stacia Keller, Steven P. DenBaars, Shuji Nakamura, and Evelyn L. Hu

Departments of Materials and Electrical & Computer Engineering, University of California—Santa Barbara, Santa Barbara, California 93106

(Received 20 May 2005; accepted 29 November 2005; published online 20 January 2006)

Photonic crystal membrane cavities play a key role as building blocks in the realization of several applications, including quantum information and photonic circuits. Thus far, there has been no work on defect cavities with active layers emitting in the UV to green range of the spectrum based on the (Al,In,Ga)N material system. While this material system has great potential for a new generation of optoelectronic devices, there are several obstacles for the fabrication of GaN-based membrane cavities, including the absence of a conventional selective chemical wet etch. Here, we demonstrate the first fabrication of fully undercut GaN photonic crystal membranes containing an InGaN multiquantum well layer, fabricated using band-gap-selective photoelectrochemical etching. A postfabrication coating of Ta₂O₅ is used to tune the cavity modes into resonance with the quantum well emission, and the fabricated membranes exhibit resonant modes with $Q=300$. © 2006 American Institute of Physics. [DOI: 10.1063/1.2166680]

Recent work on photonic crystal resonators has demonstrated the potential of these structures to achieve optical modes with high Q values within small modal volumes,^{1–3} allowing the observation of phenomena such as the Purcell effect,⁴ strong coupling,⁵ and low-threshold lasing.^{6,7} Although InGaN/GaN devices might serve as important new sources, there have been no reports of photonic crystal resonators in this material system so far. However, photonic crystals in GaN devices have been used for light extraction.^{8–12}

In this letter, we present the fabrication of GaN-based photonic crystal membrane cavities and discuss resonant modes observed in microphotoluminescence (μ -PL) spectroscopy.

The starting materials were grown by metalorganic chemical vapor deposition (MOCVD) on a (0001) sapphire substrate (Namiki Precision Jewel Co. Ltd.) on which a $\approx 2 \mu\text{m}$ thick GaN template layer was deposited. First, a five-period In_{0.04}Ga_{0.96}N/In_{0.07}Ga_{0.93}N (20 nm/20 nm) superlattice was grown which served as a sacrificial layer for subsequent photoelectrochemical (PEC) etching.^{13–16} A 20 nm Al_{0.2}Ga_{0.8}N layer was then grown, followed by 74 nm GaN. A four-period InGaN/GaN multiquantum well (MQW) (4 nm/8 nm) with an emission at $\lambda=502$ nm served as the active layer of the structure, and this was capped by a 14 nm GaN layer. The complete structure is displayed in Fig. 1(a).

The photonic crystal pattern was formed using electron-beam lithography (EBL) in a 50 kV JEOL JBX-5DII(U) EBL system. A plasma-enhanced CVD-grown SiO₂ layer (50 nm) served as a hard mask. ZEP520A (380 nm) was used on top of the SiO₂ as a resist. We fabricated an H2 defect by removing seven holes from the center of a triangular two-dimensional photonic crystal.¹⁷ The lattice constant was kept fixed at $a=200$ nm, while the r/a ratio was varied

between 0.275 and 0.375. The pattern was then transferred into the SiO₂ by reactive ion etching (RIE) in a CHF₃ plasma and subsequent RIE in a Cl₂ plasma formed the pattern in the GaN heterostructure. The etch depth was ~ 300 nm to ensure that the sacrificial layer was accessible to the electrolyte during PEC etching. The sample was then prepared for PEC etching. Circular mesas were defined around the photonic

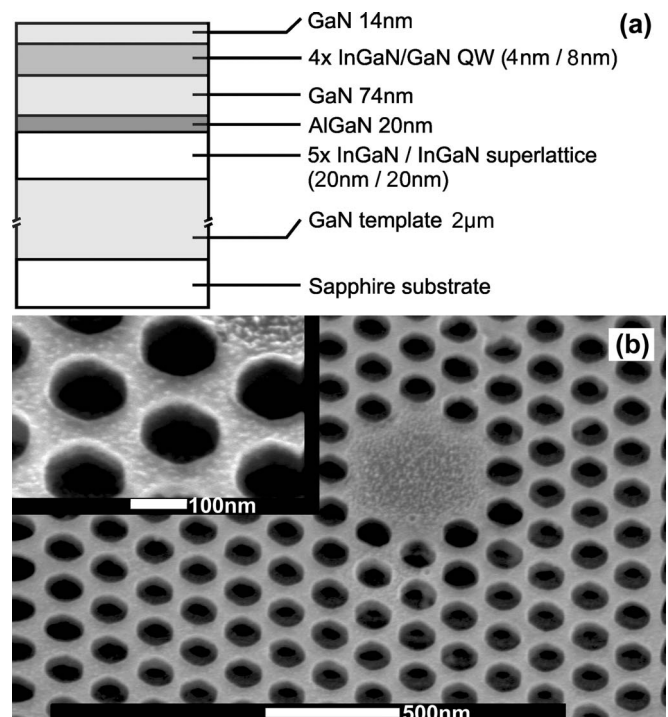


FIG. 1. (a) MOCVD-grown layer structure. The thicknesses are target values. (b) Scanning electron micrograph of a H2 photonic crystal defect cavity. The lattice constant is $a=200$ nm. Inset: Magnified detail view. Both micrographs have been taken under 30° tilt angle.

^{a)}Electronic mail: cedrik.meier@uni-duisburg.de

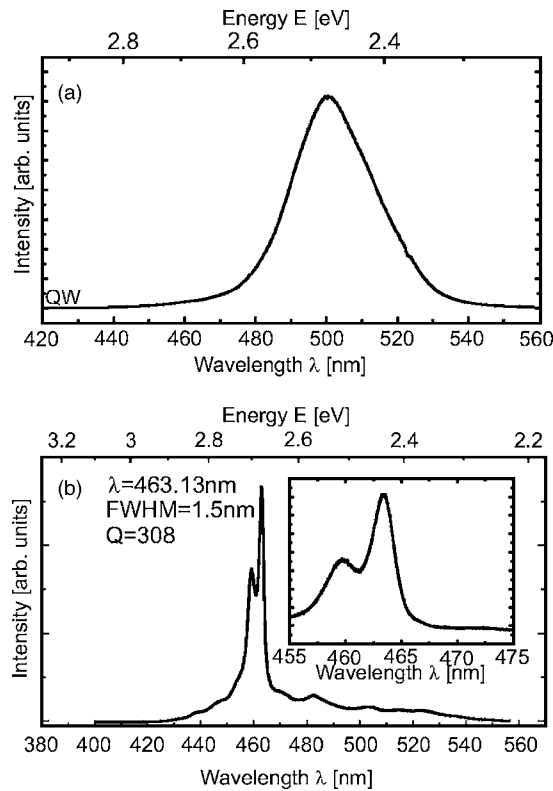


FIG. 2. Microphotoluminescence spectra taken at $T=300$ K. (a) Spectrum of the MQW sample before device fabrication. (b) Spectrum of a device showing confined modes.

crystals using contact lithography-based RIE etching. The formation of the membrane was carried out by a PEC process which selectively removed the InGa_N superlattice. The process is similar to one described in the work by Haberer *et al.*^{15,16} A Ti/Pt (15 nm/35 nm) electrode was formed around the mesas to facilitate PEC etching which was carried out in a dilute electrolyte (0.004M HCl aqueous solution) under constant agitation. The sample was illuminated using a 1000 W Xe lamp, and light with wavelengths shorter than 365 nm was filtered out using an unintentionally doped GaN filter to prevent etching of the GaN/AlGa_N layers. Lateral etch rates were around 30 nm/min. The finished device is displayed in Fig. 1(b). As can be seen, the membrane was well defined and had a total thickness of approximately 90 nm. This is thinner than the 156 nm anticipated from the material design, and has an impact on the photonic confinement. The deviation of the actual from the designed thickness may result from growth rate variations, or slight overetching of the membrane during the PEC process. Accordingly, we deposited 70 nm of Ta₂O₅ ($n=2.1$) on the devices to compensate the thin membrane thickness and to ensure a large enough photonic bandgap. The devices were characterized by room temperature microphotoluminescence measurements in confocal geometry. A cw-HeCd laser ($\lambda=325$ nm, $P=7$ mW) was used for excitation. Laser light was focused and the photoluminescence signal was collected using a refractive UV compatible microscope objective (80 \times , numerical aperture=0.55). A spot diameter around $d=3$ μ m was achieved. The spectra were taken using a Czerny-Turner monochromator ($f=0.55$ m, 1200 nm⁻¹ grating) and a CCD camera.

The spectra are displayed in Fig. 2. The emission of the MQW before fabrication is shown in Fig. 2(a). As can be

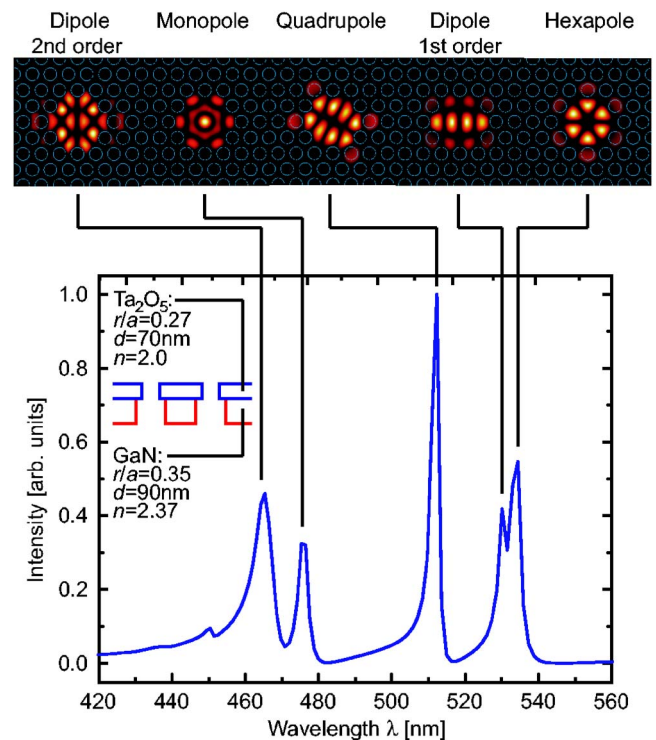


FIG. 3. Three-dimensional calculation for the H2 defect in a GaN/Ta₂O₅ membrane.

seen, the spectrum shows a broad full width at half-maximum (FWHM) [$\Delta\lambda=24$ nm] peak at $\lambda=502$ nm. In Fig. 2(b), we show a μ -PL graph for a device where confined modes could clearly be observed. At $\lambda=459.4$ and 463.0 nm, two narrow (FWHM $\Delta\lambda=1.5$ nm) spectral lines are observed. These two lines completely dominate the background quantum well emission at $\lambda=502$ nm. The observed peaks correspond to a quality factor of $Q=\lambda/\Delta\lambda=300$. As expected for a confined mode, this mode could only be excited in a small region of several 100 nm around the center of the device, and was spatially extremely sensitive. Although this is a relatively modest value of Q , given the possible strain, defects and other loss mechanisms in the material, we believe that this is a very encouraging result.

To analyze the spectra, we performed three-dimensional finite difference time domain simulations¹⁸ to determine the spectral position of resonant modes in these devices. Our findings are summarized in Fig. 3. We used a lattice constant of $a=200$ nm and assumed a 70 nm layer of Ta₂O₅ ($n=2.1$) on top of a 90 nm layer of GaN ($n=2.37$). For the hole diameters, we have used $r/a=0.35$ for the GaN and $r/a=0.27$ to adjust for slight reduction of hole diameter of the Ta₂O₅ layer during e-beam deposition. The cross section of the simulated structure is shown in the inset of Fig. 3. As a source, we have used H_z magnetic dipoles. These dipoles excite only TE-polarized modes. This is reasonable, since for the studied range of r/a the device does not support a band gap for TM modes. We assume that since the carriers in the InGa_N layers are confined in the well, they do possess a significant in-plane dipole, which can couple to TE modes.

The most striking result is that, in spite of the relatively low indices of the materials used, we find a large photonic band gap, ranging from 450 to 540 nm ($\Delta\lambda=90$ nm). We also find a number of well confined modes for this particular defect cavity. Indeed, we see six spectral features, at 450,

465, 476, 511, 530, and 534 nm. While the five modes at lower energies are defect modes, the highest-energy mode at 450 nm is the photonic band-edge mode. For the four confined modes, we also calculated the magnetic field component H_z . The results are shown in the upper part of Fig. 3. We are able to identify the hexapole, the quadrupole, the first-order dipole, and the monopole mode. The mode at 465 nm is most likely a second-order dipole mode. We conclude this from the symmetry of the field distribution for this mode if compared to the first-order dipole mode.

If we compare those results to our experimental findings, we conclude that the strongly confined modes that we observed at 460 nm are the second-order dipole mode. If we were to observe the photonic band-edge mode in our experiments rather than a confined defect mode, we should be able to excite this mode in the entire photonic crystal. However, we can only excite the confined mode in a submicron-sized spatial region in the device center. As the energy for the observed mode is rather high, it is reasonable to assume that we observe a mode in the high-energy region of the band gap. As we do see a degeneracy lifted mode, it is unlikely that we observe a monopole mode where we would not expect a splitting in energy. Therefore, it is reasonable to assume that the observed mode is indeed the second-order dipole mode from our simulations. The found deviation of 5 nm is in reasonable agreement within the limits of uncertainties in determination of hole diameters, membrane thickness, and to fabrication irregularities. These fabrication imperfections lift the double degeneracy of the second-order dipole mode and it explains why we see a double-peak feature in our PL measurements rather than a single peak. The question as to why we do not see the modes at lower energy is not easy to answer. Indeed, the calculated mode distribution (Fig. 3) does not reflect the outcoupling strength of each mode directly. Moreover, the specific device geometry will influence which modes are preferred for coupling. One might speculate if the less pronounced features experimentally found at 482 and 505 nm arise from those other modes found in the simulation.

In conclusion, we have fabricated fully undercut photonic crystal membranes with defect cavities in GaN, incorporating an InGaN multiquantum well as an active layer. We have shown that a layer of Ta₂O₅ can be used to compensate for MOCVD layer thickness inhomogeneities. The fabricated

devices show confined modes with linewidths around $\Delta\lambda = 1.5$ nm ($Q=300$). Comparison with simulations shows that these structures support a wide photonic band gap and a number of well confined modes. Further design and process optimization should substantially improve the Q values, and we expect those results to stimulate the progress on photonic devices for the visible and ultraviolet spectral region significantly.

The authors would like to thank P. M. Petroff for support with UV μ -PL spectroscopy. One of the authors (C.M.) acknowledges funding by the Deutsche Forschungsgemeinschaft under grant number ME 2087/1.

¹K. Hennessy, C. Reese, A. Badolato, C. F. Wang, A. Imamoğlu, P. M. Petroff, E. Hu, G. Jin, S. Shi, and D. W. Prather, *Appl. Phys. Lett.* **83**, 3650 (2003).

²B.-S. Song, S. Noda, T. Asano, and Y. Akahane, *Nat. Mater.* **4**, 207 (2005).

³Y. Akahane, T. Asano, B.-S. Song, and S. Noda, *Nature (London)* **425**, 944 (2003).

⁴A. Badolato, K. Hennessy, M. Atatüre, E. Hu, P. M. Petroff, and A. Imamoğlu, *Science* **308**, 1158 (2005).

⁵T. Yoshie, A. Scherer, J. Hendrickson, G. Khitrova, H. M. Gibbs, G. Ruper, C. Ell, O. B. Shchekin, and D. G. Deppe, *Nature (London)* **432**, 200 (2004).

⁶S. Strauf (unpublished).

⁷M. Loncar, T. Yoshie, A. Scherer, P. Gogna, and Q. Yueming, *Appl. Phys. Lett.* **81**, 2680 (2002).

⁸J. J. Wierer, M. R. Krames, J. E. Epler, N. F. Gardner, M. G. Craford, J. R. Wendt, J. A. Simmons, and M. M. Sigalas, *Appl. Phys. Lett.* **84**, 3885 (2004).

⁹J. Shakya, J. Y. Lin, and H. X. Jiang, *Appl. Phys. Lett.* **85**, 2104 (2004).

¹⁰T. N. Oder, J. Shakya, J. Y. Lin, and H. X. Jiang, *Appl. Phys. Lett.* **83**, 1231 (2003).

¹¹T. N. Oder, K. H. Kim, J. Y. Lin, and H. X. Jiang, *Appl. Phys. Lett.* **84**, 466 (2004).

¹²A. David, C. Meier, R. Sharma, F. Diana, S. P. DenBaars, E. L. Hu, S. Nakamura, C. Weisbuch, and H. Benisty, *Appl. Phys. Lett.* **87**, 10117 (2005).

¹³C. Youtsey, I. Adesida, and G. Bulman, *Electron. Lett.* **33**, 245 (1997).

¹⁴C. Youtsey, L. T. Romano, and I. Adesida, *Appl. Phys. Lett.* **73**, 797 (1998).

¹⁵E. D. Haberer, R. Sharma, C. Meier, A. R. Stonas, S. Nakamura, S. P. DenBaars, and E. L. Hu, *Appl. Phys. Lett.* **85**, 5179 (2004).

¹⁶E. D. Haberer, R. Sharma, A. R. Stonas, S. Nakamura, S. P. DenBaars, and E. L. Hu, *Appl. Phys. Lett.* **85**, 762 (2004).

¹⁷C. Reese, B. Gayral, B. D. Gerardot, A. Imamoğlu, P. M. Petroff, and E. Hu, *J. Vac. Sci. Technol. B* **19**, 2749 (2001).

¹⁸Commercial software provided by Lumerical Computer Solutions.